Total Lightning as an Indicator of Mesocyclone Behavior

Sarah M. Stough[1,*], Lawrence D. Carey[1], Christopher J. Schultz[1,2]

1. Department of Atmospheric Science, University of Alabama in Huntsville, Huntsville, AL, USA
2. Earth Science Office, NASA Marshall Space Flight Center, Huntsville, AL, USA

ABSTRACT:

Studies have documented the relationship between severe weather and total (in-cloud and cloud-to-ground) lightning activity, indicating that total lightning in particular may have utility for nowcasting severe weather. In order to maximize its potential in operations, total lightning data is best integrated through fusion with proven tools. As such, this study lays some of the groundwork for fusing total lightning with radar into a multi-sensor algorithm for severe weather detection and forecasting. Specifically, Weather Surveillance Radar-1998 Doppler (WSR-88D) and Lightning Mapping Array (LMA) data are analyzed for supercell thunderstorm events as an initial investigation of the concept.

In supercells, the updraft plays a pivotal role in the production of both total lightning and the storm's mesocyclone, a key signature for the prediction of severe phenomena observed at the ground. Specifically, a low-to-mid-level updraft that is responsible for cloud electrification and flash production could also contribute to the tilting of environmental horizontal vorticity into the vertical, the subsequent stretching of this vertical vorticity, and the development and intensification of a mesocyclone. Because of this physical-dynamical connection, lightning may provide an early indication of changes in updraft strength that can herald the imminent development or strengthening of a storm's mesocyclone. In turn, the mesocyclone may be used as a signal of impending severe events, as it is an indication of a storm's dynamic strength and its capability to produce hail, damaging winds, and possibly tornadoes.

Better understanding of this relationship between total lightning, mesocyclogenesis, and severe weather could assist forecasters by tipping the scales in favor of or against issuing a severe or tornado warning early in an event. Case studies of supercell storms are used to explore the hypothesis that total lightning activity can offer additional, perhaps early, insight into mesocyclone development and subsequent severe phenomena. These studies include analysis of LMA data, WSR-88D mesocyclone detection output from the operational National Severe Storms Laboratory (NSSL) Mesoscyclone Detection Algorithm (MDA), products from the Warning Decision Support Systems - Integrated Information (WDSS-II) tool, and dual-polarization radar data. Flash rates and trends from the lightning jump algorithm, a tool used to identify rapid increases in lightning, are observed alongside occurrence, strengthening, and rotational characteristics of mesocyclones and other radar-inferred properties. Using these attributes, preliminary results indicate that some relationship does exist between lightning jumps, local maxima in lightning flash rates, and development or strengthening of a storm mesocyclone that can be associated with storm severity.

INTRODUCTION

The expanding availability of total (i.e., in-cloud and cloud-to-ground) lightning data over the past several decades has allowed increased documentation of the relationship between total lightning activity and severe phenomena [e.g., Williams et al. 1999; Goodman et al. 2005; Steiger et al. 2007; Montanya et al. 2009; Schultz et al. 2009; Darden et al. 2010; Gatlin and Goodman 2010; Pineda et al. 2011; Schultz et al. 2011]. More recently, this relationship has been explored through the framework of the lightning jump, which statistically defines a rapid increase in lightning flash rate [Schultz et al. 2009; Gatlin and Goodman 2010; Schultz et al. 2011]. From related research, these definable rapid increases in total lightning flash

Contact information: Sarah M. Stough, University of Alabama in Huntsville, Department of Atmospheric Science, Huntsville, AL, USA, Email: sarah.stough@nsstc.uah.edu

rate, or lightning jumps, often precede instances of severe weather at the ground. These results indicate that lightning data may possess some operational utility in giving added awareness of storm characteristics that could bolster confidence in warning decisions and ultimately result in increased warning lead time. In order to maximize the capabilities of total lightning data for nowcasting severe storms, its fusion with proven tools has become a major goal in the research and operational communities. This is also driven by anticipated widespread total lightning detection capabilities over the Americas afforded by the Geostationary Operational Environmental Satellite Series R (GOES-R) Geostationary Lightning Mapper [Goodman et al. 2013]. As such, this study lays some of the conceptual groundwork for fusing radar with total lightning on a national level into a multi-sensor algorithm for severe weather detection and forecasting.

Work relating total lightning and severe weather is based upon the microphysical and kinematic connection between storm electrification and dynamics. In particular, the updraft plays a pivotal role in both charge separation leading to flash initiation and mesocyclogenesis, the hallmark of isolated severe convection. The primary means for cloud electrification is thought to be the rebounding collisions between graupel and ice crystals in the presence of supercooled water, or so-called non-inductive charging (NIC) [Takahashi 1978]. NIC at the particle scale is followed by storm scale charge separation due to differences in particle fall speeds and the action of a vigorous updraft. The low-to-mid-level updraft that is ultimately responsible for cloud electrification via NIC and eventual flash production also contributes to the tilting of environmental horizontal vorticity into the vertical, the subsequent stretching of this vertical vorticity, and the development and intensification of a mesocyclone [Rakov and Uman 2003; Lemon and Doswell 1979]. A quasi-steady, rotating updraft, or mesocyclone, that extends through the depth of a storm is often the primary indicator in the initial diagnosis of a severe supercell storm. Although only roughly 26% of mesocyclones have been found to be associated with tornadoes, approximately 90% of all mesocyclones are associated with severe phenomena [Stumpf et al. 1998; Trapp et al. 2005]. Despite this knowledge, challenges remain in operational nowcasting of severe weather that include correctly identifying and diagnosing the first severe storm of a convective event as well as providing advanced warning on the first tornado of the day [Brotzge and Ericksen 2009; Brotzge and Donner 2013].

The work here specifically explores the temporal relationship between strengthening supercell rotation and intensification of lightning activity objectively identified by the Schultz et al. [2009, 2011] two-sigma lightning jump. Using National Weather Service (NWS) Weather Surveillance Radar –1988 Doppler (WSR-88D) and Lightning Mapping Array (LMA) data, an initial investigation of supercell thunderstorms is conducted to determine how lightning coupled with radar-derived rotation indicators may give earlier indication of updraft strength to improve situational awareness, increase warning lead time, or potentially “tip the scales” between severe versus tornado warnings given *a priori* environmental knowledge. The next section provides additional information about the datasets used, followed by details on analysis methods. Results and interpretation are provided in the fourth section with concluding remarks and future work outlined afterward.

DATA AND INSTRUMENTATION

Total lightning data from two local LMA networks as well as archived Level II and Level III data from several S-band WSR-88D radars in the Next Generation Weather Radar (NEXRAD) network constitute the primary datasets used in this study. These data were collected from the North Alabama and Central Oklahoma regions for four separate storm case studies.

Lightning data

Total lightning data from the North Alabama Lightning Mapping Array (NALMA) and the Oklahoma Lightning Mapping Array (OKLMA) were used in this study [Goodman et al. 2005; MacGorman et al. 2008]. LMAs are local-scale networks that measure the time of arrival (TOA) of individual very high frequency (VHF) point radiation sources associated with electrical breakdown. An algorithm can be used to cluster these sources by time and location proximity factors into groups reconstructing 2- or 3-D flashes. For analysis presented here, a flash clustering algorithm similar to that described in McCaul et al.

[2005] is used. Generally, LMA stations record the time and magnitude of the peak radiation emitted from lightning in intervals of 80 μs in a local unused television channel. These measurements result in tens to hundreds of recorded source points detected per flash from multiple stations, at least six for better spatiotemporal accuracy. The combination of these time recordings and stationary positions is used to locate the emittance time and location of individual sources in a flash. For each source point, a chi^2 statistic is calculated revealing a goodness of fit and quality of the data. Together, all of these points can provide mapped sources with horizontal (vertical) location errors of less than 500 m (1000 m) within a range of 100 km of the network [Koshak et al. 2004]. Measurements have been determined to decrease in location accuracy outside of this network range, particularly for height calculations [Koshak et al. 2004].

Radar data

Data from four WSR-88D installations, KHTX in Hunstville, AL; KBMX in Birmingham, AL; KGWX in Columbus, MS; and KTLX in Twin Lakes, OK; were ordered from the National Oceanic and Atmospheric Administration (NOAA) National Climatic Data Center (NCDC) for this study. Analysis and visual interrogation are based upon radar reflectivity factor characteristics and Doppler velocity calculations, as well as the variables of differential reflectivity factor and specific differential phase where available. Crum and Alberty [1993] explain the benefits and limitations of the original NEXRAD network, which has since been upgraded to dual-polarization capabilities, documented by Doviak et al. [2000]. Dual-polarization radar is characterized by the ability to transmit electromagnetic waves and receive scattered returns in both the horizontal and vertical orientation. Because of this, more information can be obtained about the size, shape, concentration, orientation, phase, and density of targets than with horizontal reflectivity factor (Z_{HH}) alone, allowing inference of drop size distribution, particle types, and phase transition. The two polarimetric variables discussed here include differential reflectivity (Z_{DR}) and specific differential phase (K_{DP}). Simply put, Z_{DR} provides a measure of the mean axis ratio of hydrometeors in a volume, but is not dependent upon the concentration of hydrometeors, while K_{DP} is a propagation variable, indicating the differential phase shift between horizontal and vertical polarizations in a volume over a specific range. The primary difference in the two variables is that K_{DP} is affected by hydrometer shape as well as concentration. There are many foundational works that document and describe these and other variables along with their capabilities and limitations in more detail, several of which are collected in Straka et al. [2000].

Recent work utilizing polarimetric data has addressed a variety of signatures seemingly unique to supercell thunderstorms [Kumjian and Ryzhkov 2008, 2009; Romine et al. 2008, Crowe et al. 2010, 2012; Kumjian et al. 2010; Van den Broeke et al. 2010]. Two signatures, termed the Z_{DR} arc and separation of columns of Z_{DR} and K_{DP} in a storm, may in particular provide in-situ indication of how a storm modifies environmental storm relative helicity (SRH). This is based on the idea that the signatures appear as a result of size sorting of hydrometeors due to low-level wind shear. For example, a well-defined arc of Z_{DR} maxima along the forward flank downdraft (FFD) would be indicative of increased size-sorting and SRH modification. Additionally, enhanced low-level separation of Z_{DR} and K_{DP} maxima, rather than relative collocation of these maxima, is thought to be indicative of increased low-level vertical wind shear [Romine et al. 2008; Kumjian and Ryzhkov 2008, 2009; Kumjian et al. 2010; Crowe et al. 2010, 2012]. Because of these signatures and kinematic relationships, Z_{DR} and K_{DP} were employed for analysis as well.

Of the other variables discussed here, reflectivity was generally used in each case to assess storm structure for supercell characteristics. Meanwhile, Doppler velocity data were analyzed for qualities of storm-scale rotation and the presence of a mesocyclone. In addition to the variables previously discussed, two of the output product datasets from the Level III Radar Product Generator (RPG) were used. The NOAA National Severe Storms Laboratory (NSSL) Digital Mesocyclone Detection Algorithm (MDA) and Tornado Detection Algorithm (TDA), referred to in the data by product codes “NMD” and “TVS”, respectively, were chosen so that an objective definition and time history of storm rotation would be available for analysis [Mitchell et al. 1998; Stumpf et al. 1998]. While both algorithms rely upon spatial Doppler velocity constraints for identification, the MDA additionally requires persistent identification through time of rotation defined by different horizontal spatial requirements and more detailed vertical spatial constraints than the TDA. The TDA product is described in detail in Mitchell et al. [1998], while

the MDA is documented by Stumpf et al. [1998]. Only the presence of a tornado vortex signature (TVS) from the TDA output, or lack thereof, was considered in this study; however, the mesocyclone strength index (MSI) attribute from the NMD output was chosen as an analysis parameter. This attribute takes into account vertically integrated strength ranks of rotation that are computed and thresholded based on gate-to-gate Doppler velocity difference and shear [Stumpf et al. 1998].

METHODS

Four supercell storms were analyzed using the Warning Decision Support System - Integrated Information (WDSS-II) as well as other algorithms [Lakshmanan et al. 2007]. While the NMD and TVS data were already in the form of post-processed algorithm output, associating lightning flashes with storms, or tracking, calculating lightning jumps, determining a Doppler velocity-based mesocyclone proxy, and analysis of polarimetric signatures required data manipulation before combined analysis. WDSS-II was the primary toolkit for the process of associating lightning flashes with particular storms, converting Doppler velocity data into layered azimuthal shear fields, and gridding Z_{DR} and K_{DP}. After identifying the total lightning flashes associated with each storm through time, the Schultz et al. [2009] two-sigma lightning jump algorithm was implemented on the flash counts to identify lightning jumps in each storm. Polarimetric analysis for one case was done qualitatively as well as using a newly-defined K_{DP}, Z_{DR} overlap analysis technique

Lightning association and jump computation

Lightning mapping arrays produce source maps and flash maps resulting from a clustering algorithm that cover the entire LMA domain. To determine the flash rate and lightning jump associated with a particular storm, spatiotemporal boundaries must be identified for each storm to isolate its specific flashes. Using the K-Means identification and tracking algorithm described by Lakshmanan et al. [2009, 2010], storm features based on flash extent density (i.e., the number of lightning flashes that pass through an area per minute) and reflectivity are computed in WDSS-II. When flash extent density was utilized, it was derived from LMA source data to be identified and tracked. While flash extent density is exclusively a product of lightning data, it displays similar storm structure in terms of size and shape as radar reflectivity, often with clearer boundaries between storm features. Examples of this may be seen in Fig. 1. When radar reflectivity was utilized, it was first merged with surrounding local radars and gridded to a 1-km grid using the w2merger tool [Lakshmanan et al. 2006]. Then, the height at -10ºC for the case and region was identified based on a local proximity sounding, and the merged grid was tracked for storm cells at that level using the K-Means algorithm. The output from the K-Means algorithm includes spatial boundaries based on feature footprints for each storm at two-minute intervals. Flash initiation locations from flashes computed using

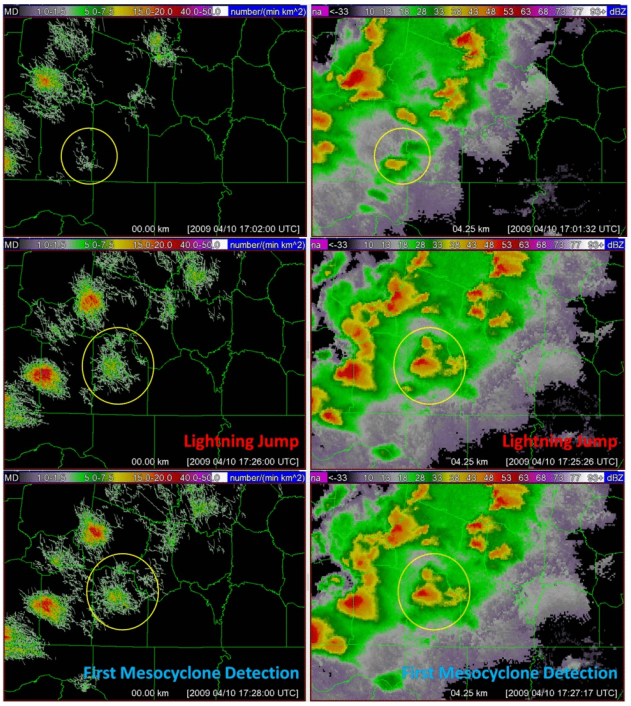

Figure 1: Flash extend density shown in left column images and reflectivity at -10ºC shown in right column images at the time the storm was first tracked (1702 UTC, first row), the time of the first lightning jump (1726 UTC, second row), and at the time of the first NMD detection (1728 UTC, third row). The storm of interest is circled in yellow in each image.

the McCaul et al. [2005] algorithm that fall within each footprint's boundary over the previous two-minute period are then said to be associated with that storm based on the K-Means algorithm output.

After lightning flashes have been associated with a particular storm, the Schultz et al. [2009, 2011] two-sigma lightning jump algorithm is applied to determine the presence of a rapid increase in flash rate. It should be noted that this algorithm requires twelve minutes of "spin-up" time so that the first flashes a storm produces are not incorrectly marked as a lightning jump. While tracking based on reflectivity can become difficult in less-isolated storm events, when tracking based on flash extent density, a storm is sometimes flashing before the tracking algorithm detects its presence. Therefore, the 12-minute rule truncates the applicable data and legitimate jumps are sometimes missed. In these cases, reflectivity is used for tracking so that a storm can be identified before it becomes electrically active and its evolution can be more fully observed.

Azimuthal shear

Couplets of relative maxima in inbound and outbound Doppler velocity data are often associated with storm mesocyclones. The azimuthal derivative of radial velocity is referred to as azimuthal shear, which can be used as a proxy for a rotating updraft, otherwise observed as a couplet. Maps of azimuthal shear through a specified depth can be computed from dealiased radial velocity fields using the WDSS-II Linear Least Squares Derivative (LLSD) algorithm [Miller et al. 2013]. These maps were produced from zero to three kilometers and from three to six kilometers to represent relative low- and mid-level storm rotation. Maximum values of azimuthal shear for each layer were then identified from the region of the storm mesocyclone for each approximate five-minute radar scan period.

Polarimetric analysis

Presently, analysis of Z_{DR} arc characteristics is best accomplished through visual inspection to address the curvature, relative maxima of data comprising the arc signature, and physical extent of the arc along the FFD of a thunderstorm. This is to be done with the understanding that the strongest SRH modification results from more enhanced size sorting, qualitatively given by more curved arcs consisting of a narrow area of maximum dB situated along a tight gradient in horizontal reflectivity [Kumjian and Ryzhkov 2009]. Also, as thresholds for what constitutes a Z_{DR} maxima vary regionally and by radar wavelength, they were subjectively chosen here to be any value at or above 2 dB, regions of which can clearly be visually differentiated from background data values. Further, when conducting the separation analysis of Z_{DR} and K_{DP}, areas of Z_{DR} greater than 2 dB generally spatially agree with areas of K_{DP} maxima greater than $2^{o}km^{-1}$, a threshold often utilized in the literature [Romine et al. 2008; Kumjian and Ryzhkov 2008, 2009; Kumjian et al. 2010; Crowe et al. 2010, 2012].

To accomplish a low-level separation analysis of Z_{DR} and K_{DP}, fields of each were gridded on 1-km constant altitude plan position indicators (CAPPIs) using the WDSS-II w2merger tool. Following the gridding of these variables, values of each field corresponding to at least 10 dBZ reflectivity are limited to the thresholds discussed above, and evaluated for percent overlap in terms of the area covered by each variable. The percent overlap of the area of these variables is normalized by the maximum overlap experienced throughout the lifetime of the storm to remove bias based on relative thresholded area size. When percentage of overlap displays smaller values, most separation is occurring and most size-sorting would be expected. Here, it is important to note that occasionally toward a downward trend in storm intensity, Z_{DR} maxima significantly diminish, making the percentage overlap artificially small. Data was evaluated for this occurrence, and marked accordingly in results presented here.

RESULTS AND DISCUSSION

Three supercells were analyzed from the Tennessee Valley/North Alabama including two of which that were tornadic. One of these storms occurred following the dual polarization upgrade to KHTX, allowing polarimetric data availability. Additionally, a supercell from Central Oklahoma is included. For the storms from the North Alabama region, WSR-88D data from the KHTX radar site was primarily

utilized as its coverage closely overlaps that of the NALMA, except where neighboring KGWX and KBMX radars better resolved the storm of interest due to its location during its lifetime. For analysis of the storm from Central Oklahoma, radar data from the KTLX site was chosen as it was closest to the storm and the center of the OKLMA network.

10 April 2009

The supercell considered on this date originated a few kilometers north of the Alabama/Tennessee state line ahead of a quasi-linear convective system approaching from the west, seen in Fig. 1. It was analyzed between 1702 UTC and 1834 UTC, during which time it propagated to the north/northeast before merging with the convective line. Although it never produced a tornado, it was associated with hail reports of up to 1.75 inches in diameter. Through the lifetime of the storm, low- and mid-level azimuthal shear trends exhibited nearly similar values as seen in Fig. 2, indicating that the maximum azimuthal shear associated with the storm was typically located near the 3-km level. The NMD MSI roughly mirrored these trends as well (Fig. 2). Also, trends in lightning flash rate replicated those of the rotation parameters well, with particularly similar trends between lightning and the layer maximum azimuthal shear values as opposed to the MSI. At 1726 UTC, the supercell produced its only objectively identified lightning jump, which was followed within ten minutes by the first associated TVS at 1731 UTC and a relative maximum in NMD MSI at 1736 UTC. This jump also preceded coincident maxima in low- and mid-level layer maximum azimuthal shear at 1739 UTC. The first mesocyclone detection at 1727 UTC occurred almost simultaneously with the first lightning jump at 1726 UTC; however, maximum azimuthal shear could be detected in low- and mid-levels 20 minutes prior to the first NMD mesocyclone detection and increased at the same rate as the flash rate. Although the lightning jump only preceded the NMD mesocyclone by a minute, it occurred several minutes prior to the maxima in rotation parameters. After mesocyclone formation, persistently high flash rates agreed with continued enhanced azimuthal shear and MSI. When the NMD gave only a single detection in the period between 1746 UTC and 1804 UTC, the slight increase in flash rate again coincided with upward trends in maximum azimuthal shear from 1751 UTC to 1758 UTC and preceded the return of a continuous automated detection of the mesocyclone.

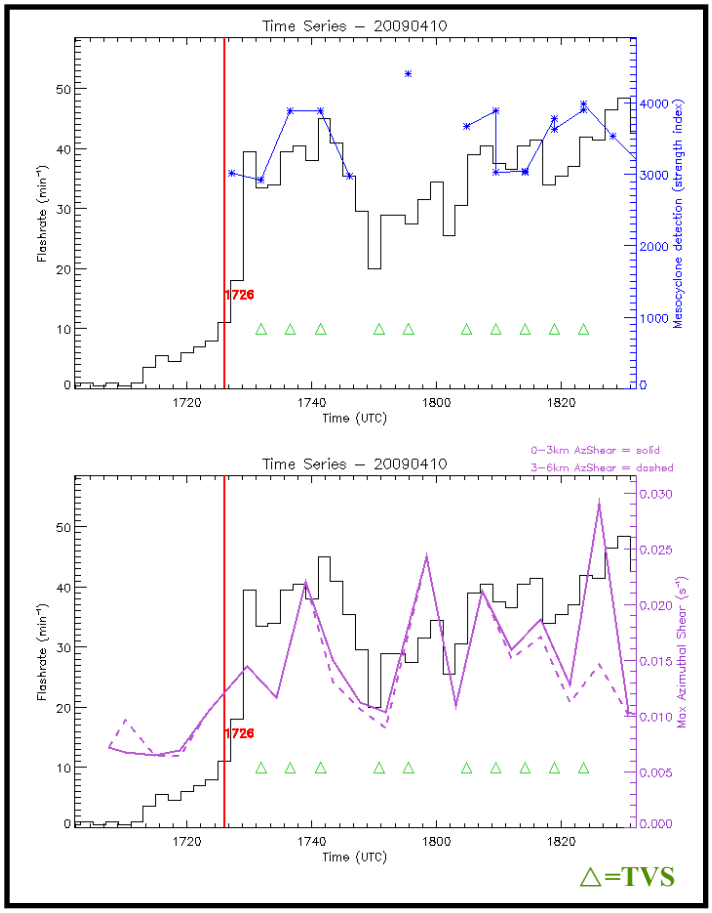

Figure 2: Time series here are shown of the supercell from 10 April 2009 in southern Tennessee. Flash rate is given in black, with trends in MSI from the NMD algorithm in blue in top image, 0-3 km maximum azimuthal shear in solid purple, and 3-6 km maximum azimuthal shear in dashed purple; both in lower image. A single lightning jump is marked in red, with TVS detections are given in green. No tornado reports are associated with this storm. Data is from the KHTX radar.

25 April 2010

This isolated supercell developed in West Central Alabama just outside of the 150 km LMA domain. After crossing into the NALMA domain, it was analyzed over two separate periods lasting from 0028 UTC to 0141 UTC (Fig. 3) and from 0220 UTC to 0401 UTC (Fig. 4) to capture different tornadic cycles. The first period encompasses two separate EF1 tornadoes, while the second covers the development of a long track EF3 tornado in eastern Alabama.

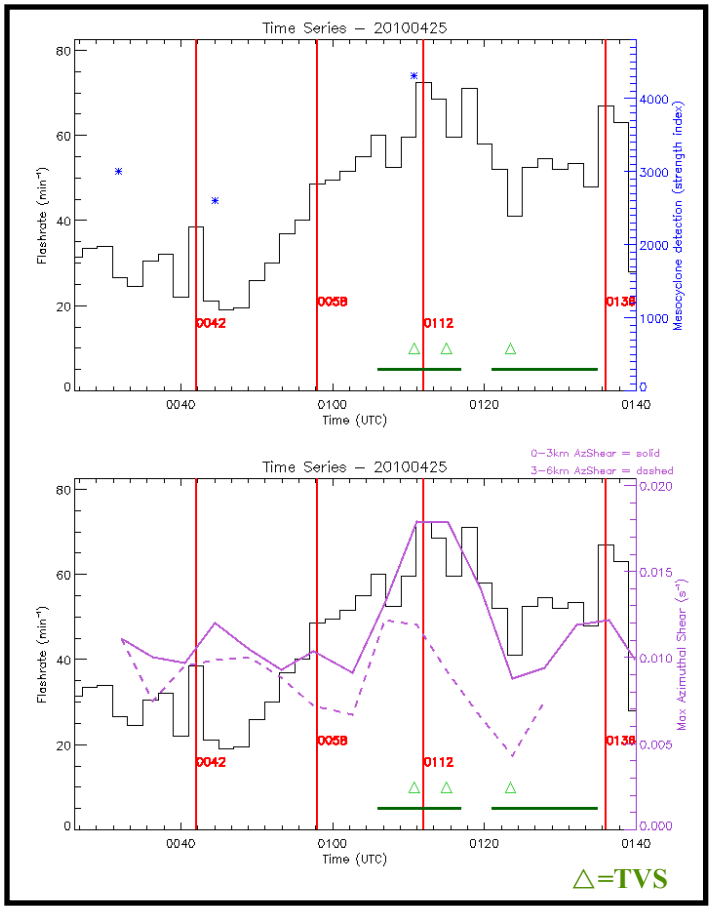

Figure 3: Time series here are shown of the first tornadic period of the storm from 25 April 2010 in Central Alabama. Data is rom the KBMX radar. Plotting is as given in Figure 2, with the addition of a solid green line representing the duration of two tornadoes reported during this period of the storm.

During the first tornadic period of the storm, the first lightning jump occurred at 0042 UTC, roughly 11 minutes after the first isolated NMD detection and 2 minutes before the second (Fig. 3). Following this jump, the NMD produced one other isolated mesocyclone detection. Meanwhile, from 0032 to 0140 UTC, the low- and mid-level layer maximum azimuthal shear exhibited nearly the same trends in lightning flash rate, with mid-level azimuthal shear maintaining values slightly below that of the low-level azimuthal shear. One minute after the low-level azimuthal shear reached a relative maximum at 0112 UTC, the second lightning jump was registered. From 0115 UTC until 0123 UTC, mesocyclone detections remained absent and the azimuthal shear measures exhibited downward trends. The first tornado was reported at 0106 UTC, eight minutes after the second jump at 0058 UTC and five minutes before the low-level layer maximum azimuthal shear peak. The third jump occurred at 0112 UTC, while the first tornado was still in progress, but preceded the second tornado report at 0121 UTC by roughly four minutes.

The second tornadic period of this storm (Fig. 4) occurred an hour after the first analysis period. The first lightning jump of the second period occurred at 0230 UTC, followed by a relative lull in lightning flash rate and azimuthal shear as well as a continued absence of mesocyclone detections. The next marked signal was the report of a tornado at 0305 UTC, over half an hour after the first identified lightning jump and five minutes prior to the next jump at 0310 UTC. The tornado also preceded the first NMD mesocyclone detection at 0309 UTC by four minutes, the first TVS detection at 0314 UTC by nine minutes, and relative maxima in low- and mid-level maximum azimuthal shear at 0316 UTC and 0321 UTC by 11 and 16 minutes, respectively. After the second jump, or reinforcing jump, at 0332 UTC during the reported tornado, the low- and mid-level azimuthal shear retain similar trends to one another, yet the low-level maximum azimuthal shear dominated while this strong, long-track tornado was on the ground. Unlike the previous two storm periods analyzed, the second storm period on 25 April 2010 was characterized by low lightning and rotation signals prior to the reported tornado. Although the classic radar signals of markedly high azimuthal shear and TVS or NMD mesocyclone detections were absent,

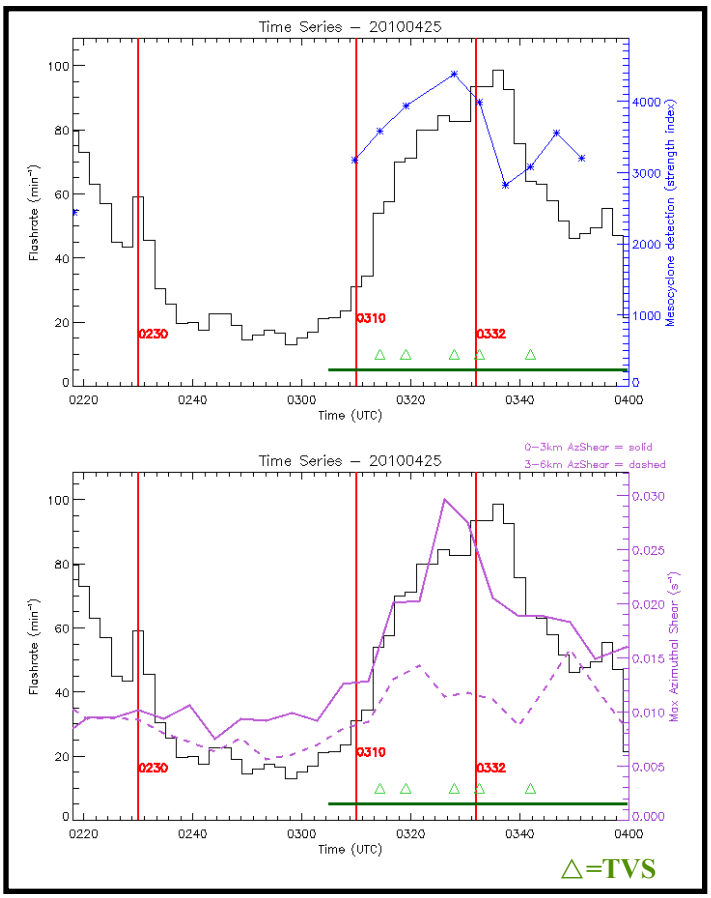

Figure 4: Time series here are shown of the second analysis period of the storm from 25 April 2010 in Central Alabama. Data is from the KHTX radar. During this time, a third tornado associated with the storm was reported. Plotting is as given in Figures 2 and 3.

the known tornadic history of the storm combined with noticeable coupled increase in lightning flash rate and azimuthal shear just prior to 0300 UTC might have given some indication that the storm could become tornadic again. In this situation, the coupled radar and lightning data along with a priori knowledge of storm behavior and environment could have given advanced notice of an increase in updraft strength and recurrent tornadic potential of this storm.

20 May 2013

From Central Oklahoma, the supercell of interest displayed slightly different characteristics than the previously described supercells. Though other storms began flashing relatively quickly, this storm almost immediately became electrically active as it became visible in radar reflectivity data. Forming in western Oklahoma, it propagated to the east/northeast over the next 90 minutes, producing a violent EF5 tornado. The first lightning jump associated with the storm was objectively identified at 1910 UTC. Because of the explosive growth of this storm, the tracking method based on flash extent density did not develop a long enough history to identify this early lightning jump. The jump was determined using semi-objective storm tracking outlined in Stano et al. [2014], and is visibly obvious in the flash rate data (Fig 5). This first jump occurred six minutes prior to the first NMD mesocyclone detection at 1916 UTC, seen in Fig. 5. Then, a second reinforcing jump at 1926 UTC occurred prior to the noticeable rise of the MSI detected at 1929 UTC; 12 minutes prior to the first TVS detection at 1938 UTC; 10 and 14 minutes prior to relative maxima in mid- and low-level layer maximum azimuthal shear at 1932 UTC and 1940 UTC, respectively; and 30 minutes before the time the tornado was first reported at 1956 UTC. Despite the 30 minute lull between the second jump and the tornado, the lightning flash rate remained unusually high at nearly two flashes per second or greater, peaking around 150 flashes per minute. Azimuthal shear values also maintained high thresholds at or above 0.02 s^{-1}. While this storm was well-forecast and may have been obviously severe with radar interrogation alone, coupling the total lightning and radar trends may have increased confidence earlier that the storm was increasing in intensity, benefitting warning decisions. Toward the end of the storm analysis period, which lasted from 1908 UTC to 2050 UTC, there was a noticeable downward trend in azimuthal shear values at low- and mid-levels, while lightning flash rates were markedly low despite the presence of a third jump. From roughly the time of 2014 UTC forward, however, the quality of lightning data were questionable due to communications issues with the network caused by electrical failure during the time the tornado impacted the OKLMA real-time data network.

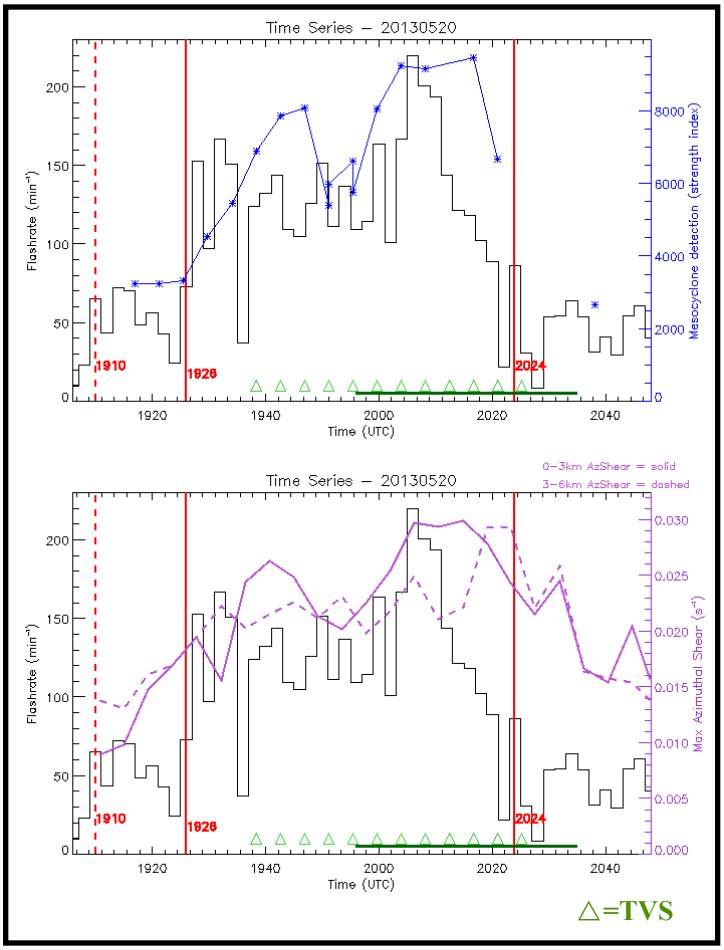

Figure 5: Time series here are shown storm from 20 May 2013 in Central Oklahoma. Data is from the KTLX radar. Plotting is as given in Figures 2 and 3. Note that the first lightning jump was determined using reflectivity to track the storm feature used for lightning association. Also, lightning data after 2014 UTC should be disregarded as quality was diminished due to tornado impacts to LMA network power and communications.

2 March 2012

This supercell, associated with the first tornado of the day in North Alabama, was part of a larger two-part severe weather event affecting much of the Ohio and Tennessee Valleys in the early morning and again later in the afternoon. This storm was tracked using the K-Means method on reflectivity at the -10ºC level, or at a 5 kilometer height, because of the limited flash production during early stages of the storm. For approximately the first hour that the storm was tracked using reflectivity, flash rates were minimal at well below 10 flashes per minute (Fig. 6). At 1438 UTC, the first lightning jump occurred, following within 8 minutes by a second and a third another 8 minutes later. The peak in flash rate occurred at 1458 UTC at 53 flashes per minute, clearly showing a rapid amplification of flash rate. All three jumps occurred between two and 18 minutes prior to the first NMD detection; however, increase in lightning flash rate during this period coincided with steadily increasing layer-maximum azimuthal shear values. The tornado, which was later rated an EF3, touched down 10 minutes before the first TVS detection at 1520 UTC, but 16 minutes after the third lightning jump in the cluster. During the time the tornado was on the ground, the NMD MSI reached a maximum at 1525 UTC. Also, the flash rates reached a relative minima as the tornadogenesis process was occurring. Similar results have been documented by Steiger et al. [2007], whose observations of decreasing flash rate approaching the time of a tornado support that a collapse of the updraft would occur prior to tornadogenesis as the downdraft intensifies. After the relative flash rate minima at 1520 UTC, a fourth jump occurred at 1632 UTC, approximately 28 minutes before the tornado lifted at 1600 UTC. Shortly before the tornado lifted, the flash rate began to rise again, but fell once more during continuously increasing layer-maximum azimuthal shear ahead of a brief minute-long tornado at 1608 UTC. After this time, the flash rates significantly decreased once again and the mid-level azimuthal shear and NMD MSI also decreased.

For this particular case, polarimetric data was available. Viewing the Z_{DR} arc evolution, the arc first appeared roughly six minutes after the first lightning jump, and lengthened along the FFD concurrently with the third lightning jump and first NMD detection at 1455 UTC (Figs. 7a-b). Three minutes after the peak flash rate occurred at 1458 UTC, the arc comparatively deepened in magnitude (Fig. 7c). At 1506 UTC, four minutes prior to the first tornado report, the arc structure weakened such that the larger Z_{DR} values extended further into the reflectivity core, indicating that the size sorting mechanism was weakening (Fig. 7d). This coincides with the weakening of the flash rate due to a reduced updraft during

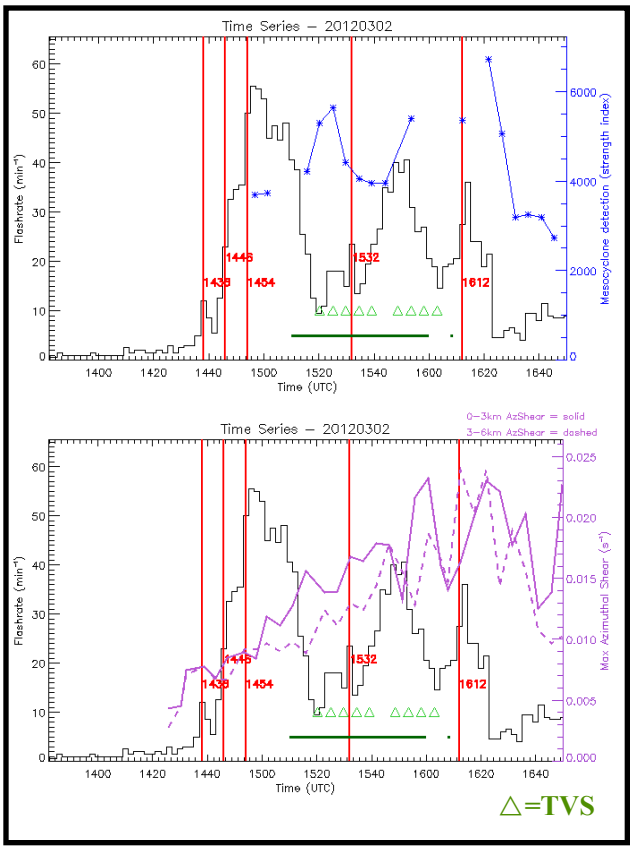

Figure 6: Time series here are shown storm from 12 March 2012 in North Alabama. Data is from the KGWX and KHTX radars. Plotting is as given in Figures 2 and 3.

tornadogenesis [Steiger et al. 2007]. At 1510 UTC, the Z_{DR} arc began to regenerate and by 1515 UTC once again extended along the periphery of the forward flank downdraft. At 1534 UTC, two minutes after the fourth lightning jump, the Z_{DR} arc reached its maximum values over its lifespan, at four or greater dB (Fig. 7e). The arc remained well-defined along the forward flank downdraft through 1544 UTC, but at 1548 UTC, it began to weaken in magnitude as the lightning flash rate once again decreased before the second brief tornado. By 1558 UTC the arc did not extend far along the forward flank downdraft, but strengthened in magnitude to include values of three to four dB. From this point forward, the arc showed slow signs of weakening, until the microphysics were obscured by the storm to the southeast overtaking this supercell. By 1640 UTC, the Z_{DR} arc had disappeared from this storm (Fig. 7f).

Low-level separation of K_{DP} and Z_{DR} was also analyzed. The moment where the storm was first close enough to KHTX such that variables could be gridded at a height of one kilometer is 1501 UTC. Also at this point, the maximum K_{DP} and Z_{DR} areas were fairly overlapped. Over the next 15 to 20 minutes, the overlap percentage rapidly decreased, reaching a relative minimum at 1516 UTC, just six minutes following tornado touchdown (Fig. 8). Despite fluctuations, the maxima separation remained greatest during the time that the tornado was on the ground. While the K_{DP} and Z_{DR} separation and flash rates tended to trend similarly for the first thirty minutes, the minima in overlap of polarimetric maxima and the peaks in flash rate begin to occur nearly simultaneously. This is first noticed with increased separation occurring at 1529 UTC, shortly after a peak in flash rate at 1524 UTC. It happens again with a flash rate peak at roughly 1550 UTC followed by increased separation at 1553 UTC and increased separation at 1613 UTC followed by a flash rate peak at 1614 UTC. While this may imply that updraft surges enhancing the flash rate may have occurred nearly simultaneously with increased low-level shear enhancements, more storm flow analysis is required.

From the polarimetric analysis, lightning seems to trend with features of the development of the polarimetric signatures throughout the storm. Whereas lightning flash rate increases and associated jumps occur prior to Doppler velocity-indicated increases in mesocyclone strength, the flash rate seems to trend simultaneously with the evolution of polarimetric signatures and their associated low-level shear and helicity implications.

CONCLUSION

The present study examines four supercell storms in a preliminary evaluation of how trends in lightning flash rate may be related to mesocyclone and storm rotation evolution. The outcome of this and future work will ultimately contribute to development of concepts for a fused radar-lightning algorithm for enhanced nowcasting. The parameters used for the lightning and mesocyclone analysis here include total

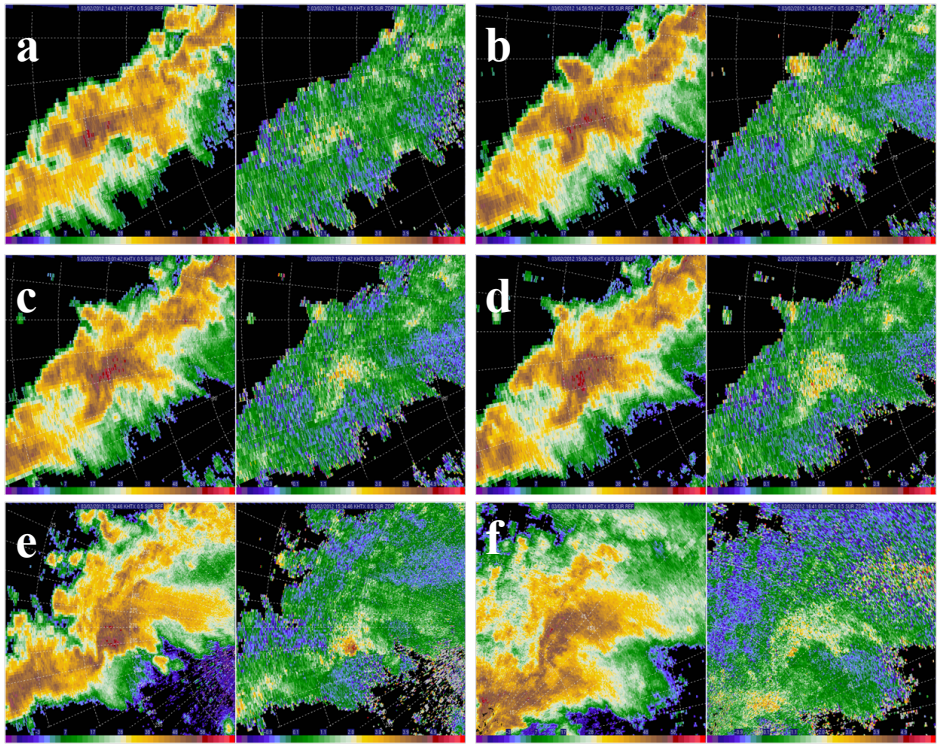

Figures 7a-f: Reflectivity (dBZ) and ZDR (dB) are shown at a 0.5 degree elevation from KHTX, shaded as shown. Scans at 1442 UTC, 1456 UTC, 1501 UTC, 1506 UTC, 1534 UTC, and 1641 UTC are provided. In Fig. 7a, Z_{DR} arc was first noticeable at 1442 UTC. At 1456 UTC, this feature had elongated along the forward flank downdraft, displaying more classic ZDR arc characteristics (Fig. 7b). At 1501 UTC, the ZDR arc had begun to intensify, showing values of three to four dB, but began eroding into the reflectivity core at 1506 UTC (Figs. 7c and 7d). At 1534 UTC, the ZDR arc displayed its maximum values(Fig. 7e). By 1641 UTC, the ZDR arc had weakened significantly (Fig. 7f).

flash rate with the lightning jump as a measure of rapid increase in lightning intensity and enhancement of storm mesocyclones given by NMD MSI, the proxy of layer maximum azimuthal shear, and SRH indications based on polarimetric signatures. Recurring elements in this analysis include similar trending in lightning flash rate and low-level layer maximum azimuthal shear, as well as midlevel layer maximum azimuthal shear to a lesser extent. Further, increased lightning activity denoted by a lightning jump often occurred simultaneously or slightly before the first mesocyclone detections given by the NMD, and prior to TVS detections. Tornadoes reported in this study were not always preceded by a lightning jump or even a mesocyclone detection or TVS. Rather, only a simultaneous upward trend in lightning flash rate and layer maximum azimuthal shear were noted prior to one tornado report in a supercell with tornadic history. In a separate storm, flash rate peaked and then dramatically declined shortly before the reported tornado, possibly indicating the breakdown of the updraft in the process of tornadogenesis. In instances such as these, it is possible that lightning data reinforcing standard radar metrics of rotation with added updraft strength information may increase forecaster confidence in perception of storm severity, especially given prior knowledge of a storm's behavior and the environment.

In terms of the polarimetric evolution in one case, decreases in flash rate seemed to occur alongside the erosion of the Z_{DR} arc signature, particularly leading to the time of the reported tornados. This is likely symbolic of the weakening of the updraft in response to the tornadogenesis mechanism. The Z_{DR} arc also

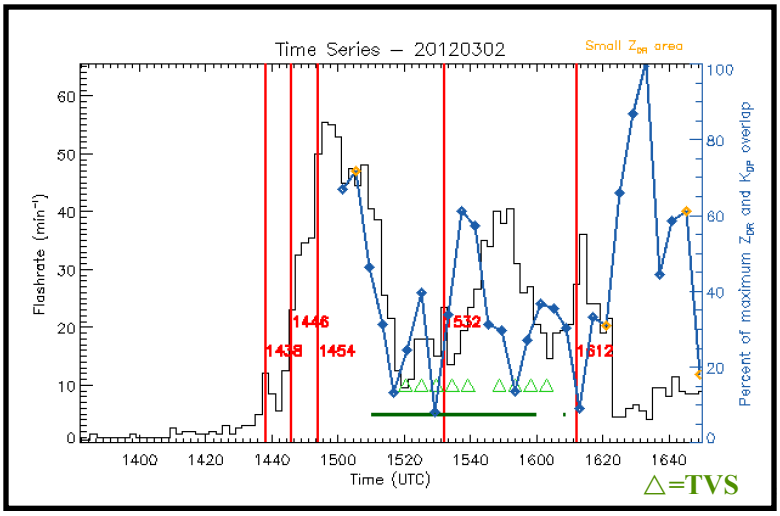

Figure 8: Time series of lightning flash rate with respect to the normalized percent of overlap of K_{DP} and Z_{DR} maxima above 2ºkm^{-1} and 2 dB, respectively. As before, total lightning flash rate is plotted in black with lightning jumps marked in red. The tornadic period is denoted by a solid green line, with green triangles representing TVS detections. The percentage of overlap of the polarimetric regions is given in blue. Times when a low area of maximum Z_{DR} was noted are marked in orange.

reached maximum values and greatest curvature and/or extent within a few minutes of lightning jumps, likely linked by the strengthening of the updraft. Further, analysis of separation of low-level K_{DP} and Z_{DR} maxima during the storm revealed that most separation occurred during the time of the reported tornadoes. Maximum separation then occurred within minutes of the relative maxima in flash rate during and after the tornado. Further analysis will be necessary to determine the dynamic and kinematic roles in these recurring trends.

It is important to note that lightning is primarily a mid-level process that may not be able to elucidate many complex low-level processes leading to tornadogenesis in supercells. However, lightning can allude to rapid updraft strengthening or weakening which can then provide a useful estimate of storm severity potential when combined with Doppler radar velocity indications of rotation. While these preliminary results show that lightning flash rate and mesocyclone behavior trend similarly, possibly as a result of the common factor of the updraft, more analysis of other parameters, such as polarimetric variables treated here, should be considered to better understand the physical link. Whereas lightning flash rate increases and jumps occur prior to increases in mesocyclone strength in all storms shown here, the flash rate seems to trend with the polarimetric evolution based on the common link of the updraft in the final storm analyzed. This may be due to its role on hydrometeor trajectories in the storm.

Plans for future investigation include further study of the storm-modified storm relative helicity evidenced by the evolving polarimetric signatures, namely the Z_{DR} arc and separation of low-level K_{DP} and Z_{DR} maxima with respect to tornadogenesis. This may elucidate whether there are other observable trends between low- and mid-level processes discussed in part here that a forecaster may benefit from. Other lightning characteristics, such as the IC to CG ratio, as well as inclusion of a larger sample of more regionally diverse tornadic and non-tornadic supercells will offer additional insight into the merit of these early results as well.

ACKNOWLEDGMENTS

The work is supported by NOAA/NASA GOES-R GLM Risk Reduction Research (R3). We thank Dr. Steven Goodman, Senior (Chief) Scientist, GOESR System Program, for his guidance and support throughout this work.

REFERENCES

Brotzge, J., S. Erickson, 2009: NWS tornado warnings with zero or negative lead times. *Wea. Forecasting*, **24**, 140–154. doi: http://dx.doi.org/10.1175/2008WAF2007076.1

Brotzge, J., W. Donner, 2013: The tornado warning process: A review of current research, challenges, and opportunities. *Bull. Amer. Meteor. Soc.*, **94**, 1715–1733. doi: http://dx.doi.org/10.1175/BAMS-D-12-00147.1

Crowe, C. C., W. A. Petersen, L. D. Carey, and D. J. Cecil, 2010: A dual-polarization investigation of tornado-warned cells associated with Hurricane Rita (2005). *Electronic J. Operational Meteor.*, **EJ4**.

Crowe, C. C., C. J. Schultz, M. Kumjian, L. D. Carey, and W. A. Petersen, 2012: Use of dual-polarization signatures in diagnosing tornadic potential. *Electronic J. Operational Meteor.,* **13**, 57-78.

Crum, T. D., R. L. Alberty, 1993: The WSR-88D and the WSR-88D operational support facility. *Bull. Amer. Meteor. Soc.*, **74**, 1669–1687.

Darden, C. B., D. J. Nadler, B. C. Carcione, R. J. Blakeslee, G. T. Stano, D. E. Buechler, 2010: Utilizing total lightning information to diagnose convective trends. *Bull. Amer. Meteor. Soc.*, **91**, 167–175. doi: http://dx.doi.org/10.1175/2009BAMS2808.1

Doviak, R. J., V. Bringi, A. Ryzhkov, A. Zahrai, D. Zrnić, 2000: Considerations for polarimetric upgrades to operational WSR-88D radars. *J. Atmos. Oceanic Technol.*, **17**, 257–278. doi: http://dx.doi.org/10.1175/1520-0426(2000)017<0257:CFPUTO>2.0.CO;2

Gatlin, P. N., S. J. Goodman, 2010: A total lightning trending algorithm to identify severe thunderstorms. *J. Atmos. Oceanic Technol.*, **27**, 3–22. doi: http://dx.doi.org/10.1175/2009JTECHA1286.1

Goodman, S. J., and Coauthors, 2005: The North Alabama Lightning Mapping Array: Recent severe storm observations and future prospects. *Atmos. Res.*, **76,** 423–437.

Goodman, S. J., R. J. Blakeslee, W. J. Koshak, D. Mach, J. Bailey, D. Buechler, L. Carey, C. Schultz, M. Bateman, E. McCaul Jr., G. Stano, 2013: The GOES-R Geostationary Lightning Mapper (GLM). *Atmos. Res.*, **125-126**, 34-49.

Koshak, W. J., and Coauthors, 2004: North Alabama Lightning Mapping Array (LMA): VHF source retrieval algorithm and error analyses. *J. Atmos. Oceanic Technol.*, **21,** 543–558.

Kumjian, M. R., A. V. Ryzhkov, 2008: Polarimetric signatures in supercell thunderstorms. *J. Appl. Meteor. Climatol.*, **47**, 1940–1961. doi: http://dx.doi.org/10.1175/2007JAMC1874.1

Kumjian, M. R., A. V. Ryzhkov, 2009: Storm-relative helicity revealed from polarimetric radar measurements. *J. Atmos. Sci*., **66**, 667–685. doi: http://dx.doi.org/10.1175/2008JAS2815.1

Kumjian, M. R., A. V. Ryzhkov, V. M. Melnikov, T. J. Schuur, 2010: Rapid-scan super-resolution observations of a cyclic supercell with a dual-polarization WSR-88D. *Mon. Wea. Rev.*, **138**, 3762–3786. doi: http://dx.doi.org/10.1175/2010MWR3322.1

Lakshmanan, V., K. Hondl, and R. Rabin, 2009: An efficient, general-purpose technique for identifying storm cells in geospatial images. *J. Ocean. Atmos. Tech.*, **26**, 523-537. doi: http://dx.doi.org/10.1175/2008JTECHA1153.1

Lakshmanan, V., and T. Smith, 2010: An objective method of evaluating and devising storm tracking algorithms. *Wea. and Forecasting*, **29**, 721-729. doi: http://dx.doi.org/10.1175/2009WAF2222330.1

Lakshmanan, V., T. Smith, K. Hondl, G. J. Stumpf, A. Witt, 2006: A real-time, three-dimensional, rapidly updating, heterogeneous radar merger technique for reflectivity, velocity, and derived products. *Wea. Forecasting*, **21**, 802–823. doi: http://dx.doi.org/10.1175/WAF942.1

Lakshmanan, V., T. Smith, G. J. Stumpf, and K. Hondl, 2007: The warning decision support system—Integrated information. *Wea. Forecasting*, **22,** 596–612.

Lemon, L. R., C. A. Doswell, 1979: Severe thunderstorm evolution and mesocyclone structure as related to tornadogenesis. *Mon. Wea. Rev.*, **107**, 1184–1197.

MacGorman, D. R., W. David Rust, T. J. Schuur, M. I. Biggerstaff, J. M. Straka, C. L. Ziegler, E. R. Mansell, E. C. Bruning, K. M. Kuhlman, N. R. Lund, N. S. Biermann, C. Payne, L. D. Carey, P. R. Krhebiel, W. Rison, K. B. Eack and W. H. Beasley, 2008: TELEX The Thunderstorm Electrification and Lightning Experiment. *Bull. Amer. Meteor. Soc.*, **89**, 997–1013.

McCaul, E. W., J. Bailey, J. Hall, S. J. Goodman, R. Blakeslee, and D. E. Buechler, 2005: A flash clustering algorithm for North Alabama Lightning Mapping Array data. Preprints, *Conf. on Meteorological Applications of Lightning Data,* San Diego, CA, Amer. Meteor. Soc., 5.2. [Available online at http://ams.confex.com/ams/Annual2005/techprogram/paper_84373.htm].

Miller, Madison L., Valliappa Lakshmanan, Travis M. Smith, 2013: An automated method for depicting mesocyclone paths and intensities. *Wea. Forecasting*, **28**, 570–585. doi: http://dx.doi.org/10.1175/WAF-D-12-00065.1

Mitchell, E. D., S. V. Vasiloff, G.J. Stumpf, A. Witt, M. D. Eilts, J. T. Johnson, K. W. Thomas, 1998: The National Severe Storms Laboratory Tornado Detection Algorithm. *Wea. Forecasting*, **13**, 352–366.

Montanya, J., S. Soula, N. Pineda, O. van der Velde, P. Clapers, G. Sola, J. Bech, and D. Romero (2009), Study of the total lightning activity in a hailstorm, *J. Atmos. Res.*, **91**, 430-437. doi:10.1016/j.atmosres.2008.06.008.

NOAA National Severe Storms Laboratory, cited 2014: NSSL research tools: Oklahoma Lightning Mapping Array. [Available online at: https://www.nssl.noaa.gov/tools/oklma/]

Pineda, N., J. Bech, T. Rigo, J. Montanyà. (2011) A Mediterranean nocturnal heavy rainfall and tornadic event. Part II: Total lightning analysis. *Atmospheric Research* **100**:4, 638-648. doi:10.1016/j.atmosres.2010.10.027.

Rakov, V. A., and M. A. Uman, 2003: *Lightning: Physics and Effects.* Cambridge University Press, 687 pp.

Romine, G. S., D. W. Burgess, and R. B. Wilhelmson, 2008: A dual-polarization-radar-based assessment of the 8 may 2003 oklahoma city area tornadic supercell. *Mon. Wea. Rev.*, **136**, 2849-2870.

Schultz, C. J., W. A. Petersen, L. D. Carey, 2009: Preliminary development and evaluation of lightning jump algorithms for the real-time detection of severe weather. *J. Appl. Meteor. Climatol.*, **48**, 2543–2563. doi: http://dx.doi.org/10.1175/2009JAMC2237.1

Schultz, Christopher J., Walter A. Petersen, Lawrence D. Carey, 2011: Lightning and severe weather: A comparison between total and cloud-to-ground lightning trends. *Wea. Forecasting*, **26**, 744–755. doi: http://dx.doi.org/10.1175/WAF-D-10-05026.1

Stano, G. T., C. J. Schultz, L. D. Carey, D. R. MacGorman, and K. C. Calhoun, 2014: Total lightning observations and tools for the 20 May 2013 Moore, Oklahoma supercell. *J. Operational Meteor.*, in press.

Straka, Jerry M., Dusan S. Zrnić, Alexander V. Ryzhkov, 2000: Bulk Hydrometeor Classification and Quantification Using Polarimetric Radar Data: Synthesis of Relations. *J. Appl. Meteor.*, **39**, 1341–1372. doi: http://dx.doi.org/10.1175/1520-0450(2000)039<1341:BHCAQU>2.0.CO;2

Steiger, S. M., R. E. Orville, and L. D. Carey, 2007: Total lightning signatures of thunderstorm intensity over north Texas. Part I: Supercells. *Mon. Wea. Rev.*, **135,** 3281–3302. doi: http://dx.doi.org/10.1175MWR3472.1

Stumpf, G. J., A. Witt, E. D. Mitchell, P. L. Spencer, J. T. Johnson, M. D. Eilts, K. W. Thomas, D. W. Burgess, 1998: The National Severe Storms Laboratory Mesocyclone Detection Algorithm for the WSR-88D*. *Wea. Forecasting*, **13**, 304–326.

Takahashi, T., 1978: Riming electrification as a charge generation mechanism in thunderstorms. *J. Atmos. Sci.*, **35**, 1536-1548.

Trapp, R. J., G. J. Stumpf, K. L. Manross, 2005: A reassessment of the percentage of tornadic mesocyclones. *Wea. Forecasting*, **20**, 680–687. doi: http://dx.doi.org/10.1175/WAF864.1

Van den Broeke, M. S., J. M. Straka, and E. N. Rasmussen, 2008: Polarimetric radar observations at low levels during tornado life cycles in a small sample of classic southern plains supercells. *J. Appl. Meteor.*, **47**, 1232-1247.

Williams, E. R., and Coauthors, 1999: The behavior of total lightning activity in severe Florida thunderstorms. *Atmos. Res.*, **51,** 245–265.